Nonequilibrium Response of the Global Ocean to the 5-Day Rossby–Haurwitz Wave in Atmospheric Surface Pressure

RUI M. PONTE*

Groupe de Recherche de Géodésie Spatiale, UMR 5566, Laboratoire CNRS-CNES-UPS, Toulouse, France

(Manuscript received 19 June 1996, in final form 24 March 1997)

ABSTRACT

The response of the global ocean to the surface pressure signal associated with the well-known 5-day Rossby–Haurwitz atmospheric mode is explored using analytical and numerical tools. Solutions of the Laplace tidal equations for a flat-bottom, globe-covering ocean, point to a depth-independent nonequilibrium response related to the near-resonant excitation of the barotropic oceanic mode. Numerical experiments with a shallow-water model illustrate the effects of realistic continental boundaries, topography, and dissipation on the solutions. The character of the oceanic adjustment and the structure of resonances changes substantially, but a nonequilibrium response occurs in all cases studied. Besides the excitation of large-scale vorticity modes or waves, which becomes less important when topography and strong dissipation are present, basin-scale nonequilibrium signals are associated with gravity wave dynamics and the process of interbasin mass adjustment in the presence of global-scale forcing and continents that require interbasin mass fluxes to occur through the Southern Ocean. Solutions with forcing most representative of the observed atmospheric wave agree qualitatively with the results of analyses of Pacific and Atlantic tide gauge records by Luther and Woodworth et al. The observed nonequilibrium signals thus seem related to the Rossby–Haurwitz forcing mode.

1. Introduction

A number of recent theoretical, numerical, and observational studies (e.g., Ponte 1992, 1993; Fu and Pihos 1994; Gaspar and Ponte 1997; Wunsch and Stammer 1997; and references therein) have indicated that at periods longer than a couple of days, most of the pressure-driven sea level variability is isostatic in nature, in agreement with a simple equilibrium or inverted barometer (IB) response in which

$$\zeta^{ib} = \frac{1}{\rho g}(\overline{p_a} - p_a). \tag{1}$$

Here, ρ is surface density, g is the acceleration of gravity, and p_a is local atmospheric pressure and $\overline{p_a}$ the spatial average of p_a over the global ocean. A remarkable exception to the tendency for static response is observed, however, for periods around 5 days. The singular character of the relation between sea level (ζ) and p_a at these periods was apparently first documented by Groves and Hannan (1968) using tide gauge records in the western Pacific, but its large-scale nature was only realized later by Luther (1982). The extensive array of tide gauges across the Pacific Ocean analyzed by Luther revealed gains of ζ on p_a for the 4–6 day band systematically different than 1 cm/mbar—the value expected for an IB response. The ζ signals were spatially coherent over the basin, with phases suggesting more or less uniform westward propagation. In addition, sea level was significantly coherent with p_a in general, but not with local winds.

Luther realized that the apparent dynamic response to p_a at 4–6 days could be related to the existence of a large-scale global oscillation in barometric pressure, which had been described in detail by Madden and Julian (1972), among others. The observed oscillation closely resembles the Rossby–Haurwitz wave solution of the Laplace tidal equations (LTE) (e.g., see Holton 1975), albeit shifted in frequency. It has a period of 5 days, zonal wavenumber $s = -1$ (westward propagating), and meridional structure given approximately by

$$\frac{3}{2}\mu P_2^1(\mu) - \frac{1}{3}P_3^1(\mu), \tag{2}$$

where μ is cosine of colatitude and P_n^l denote associated Legendre functions of degree n and order l. Maximum amplitudes of approximately 1 mbar occur at midlatitudes (Fig. 1).

Based on the different zonal wavenumbers of the forcing and response, the large-scale coherence of the re-

* On leave from Atmospheric and Environmental Research, Inc., Cambridge, MA.

Corresponding author address: Dr. Rui M. Ponte, Atmospheric and Environmental Research, Inc., 840 Memorial Drive, Cambridge, MA 02139-3794.
E-mail: ponte@aer.com

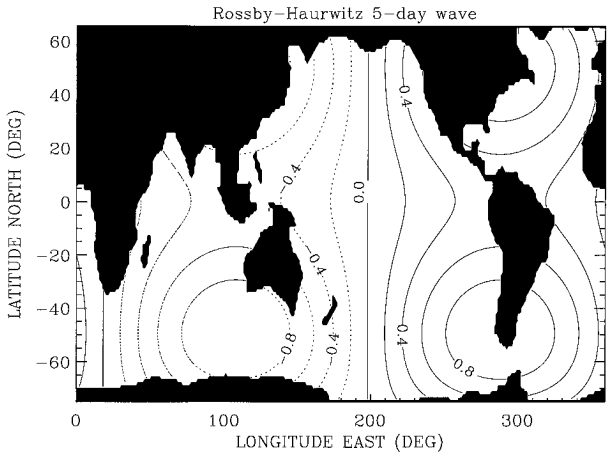

FIG. 1. Spatial structure of the 5-day Rossby–Haurwitz wave in atmospheric surface pressure described by Madden and Julian (1972). Meridional structure is given in (2) and units are millibars. Wave is shown only over oceanic domain for which numerical solutions are later considered.

sponse, and the lack of equatorial trapping of the sea level signals, Luther speculated that the dynamic response could be related to the excitation of one or more barotropic normal modes of the Pacific basin, most likely involving planetary waves and vorticity dynamics. The observed gains of ζ on p_a were mostly smaller than 1 cm/mbar, suggesting, in case of resonance, a weak excitation or highly damped response. Estimates of the dissipation based on the bandwidth of the ζ spectral peak, seen only in some of the tide gauges, and on the assumption of a single resonance in the response, indeed suggested an energy e-folding decay scale of approximately 3 days.[1] For such high damping rates, however, the establishment of basin modes, dependent on reflection of energy from boundaries, seems unlikely. More localized modes dependent on vortex stretching associated with specific topographic features are also a possibility, but in such case the large-scale coherence of ζ signals seems difficult to explain.

Another interpretation of the broad spectral bandwidth, without invoking such high dissipation rates, involves the presence of more than one resonance in the response. Miller (1989) found four vorticity modes in the 4–6 day band in his calculations of the barotropic planetary oscillations of the Pacific Ocean. In the presence of continental shelves and other finescale topography, these modes are likely to suffer some finesplitting (Miller 1986), giving rise to families of modes closely spaced in frequency, with similar large-scale structures away from relevant topographic features. Miller (1989) suggested that these modes could play a role in the observed broadband oceanic response.

Recent analysis of sea level records at St. Helena and Ascension Islands, in the tropical South Atlantic, have revealed clear departures from the IB model near a period of 5 days (Woodworth et al. 1995). Not only are the gains quite different than 1 cm/mbar at these sites, but ζ and p_a are almost in phase rather than out of phase as expected for an equilibrium response. Besides pointing to the global nature of the phenomenon, the findings of Woodworth et al. reopen the question regarding the nature of the dynamic signals. Could these signals be related after all to one or more global barotropic modes with significant amplitudes in both Pacific and Atlantic basins? The question is more than academic, as the excitation of normal modes and their observability could provide insight into barotropic ocean dynamics, including reflectivity of boundaries and dissipation processes (e.g., see Luther 1983).

To understand the dynamics behind the 5-day sea level fluctuations and help interpret the records, we examine the response of a shallow-water, barotropic, global model to pressure fields representative of the Rossby–Haurwitz atmospheric wave. Besides trying to establish if the observed ζ signals are indeed related to the Rossby–Haurwitz forcing wave, we examine the conditions under which a dynamic response is expected and the extent to which excitation of near-resonances is part of the dynamics. To introduce the numerical solutions, we first use the LTE formalism to discuss what is expected theoretically for a flat-bottom ocean covering the globe. The effects of topography, realistic geometry, and dissipation are then studied numerically and solutions compared to the tide gauge records. Our results suggest that, besides possible contributions from near-resonant excitation of basin vorticity modes, the large-scale nonequilibrium response is closely related to gravity wave dynamics and the difficulty in establishing interbasin adjustment of the mass field, in the presence of global-scale high-frequency forcing and continental land masses that force cross-basin mass shifts to occur largely through the Southern Ocean.

2. Theoretical considerations

Given a well-defined atmospheric pressure signal, it is useful to explore what is the expected nature of the oceanic response (static or dynamic?) and its vertical structure (barotropic, baroclinic, or surface trapped?) based on purely theoretical grounds. Note that our forcing wave has spatial scales large compared to the oceanic Rossby radius of deformation and a propagation phase speed of approximately 100 m s^{-1} approaching that of oceanic gravity waves and comparable to that of nondispersive (β plane) barotropic Rossby waves. Simple theoretical arguments suggest that under such conditions a dynamic response can occur (Ponte 1993). To

[1] The presence of a broadband peak in sea level need not involve any oceanic resonance, given that the atmospheric forcing itself shows a broadband peak centered at 5 days (see Fig. 5 of Luther 1982). However, the extent to which peaks in the forcing are due to the 5-day Rossby–Haurwitz mode or other shorter-scale variability, and their relation to the oceanic response, remains unclear.

be more quantitative, we consider briefly the case of a water-covered globe (no landmasses) forced by the oscillation in p_a. The exercise is also relevant to assert the effect of continents on the response, when numerical solutions are considered later.

The global nature of the forcing requires the use of the LTE over the sphere, whose free solutions are discussed in great detail by Longuet-Higgins (1968). In general, for a resting basic-state ocean with constant depth H, solutions consist of zonally propagating waves of the form $e^{i(s\psi-\sigma t)}$ and meridional structure given by the so-called Hough modes (combination of associated Legendre functions). These modes constitute a complete orthogonal set that can be used to expand the meridional dependence of any forcing field. The method of solution for the p_a forcing case thus follows closely that of the equatorial β plane (Ponte 1992) and is only outlined here; see also Holton (1975) for a detailed treatment of the stratified LTE and Longuet-Higgins (1968) for a brief discussion of the forced LTE problem.

The vertical structure of solutions for constant buoyancy frequency N is proportional to (Ponte 1992)

$$\cosh m(z + H), \tag{3}$$

where m is a vertical scale defined in terms of the equivalent depth h' as

$$m^2 = -\frac{N^2}{gh'}, \tag{4}$$

and related to s, σ, and Hough mode number j by a dispersion relation. On the equatorial β plane, an analytical form for the dispersion relation exists, but for the LTE it has to be found numerically for general h' (Longuet-Higgins 1968). In the forced problem, s and σ are fixed (and equal to the forcing parameters), defining h' for each mode j onto which the meridional structure of the forcing has a nonzero projection. In our case, the observed forcing structure is approximately a Hough mode ($j = 1$) and one expects a dominant contribution from that mode on the modal projection. Values of h' can be positive or negative, corresponding respectively, to oscillatory or evanescent dependence in z, as seen from (3) and (4).

Using the dispersion relation plotted in Figs. 2b and 17b of Longuet-Higgins (1968), one can infer the vertical scale m^{-1} for the case $s = -1$, $\sigma/2\Omega = 0.1$ corresponding to the westward propagating forcing wave of interest. (Note that, in Longuet-Higgins convention, s is always positive and the sign of σ defines zonal propagation direction. Also the values in Longuet-Higgins are presented for a sphere of unit radius. Thus, to calculate the vertical scale m^{-1} using (4), we multiply his value of $\sqrt{gh'}/2\Omega$ by $2\Omega a/N$ with a being the earth's radius.) For a typical depth-averaged value of $N = 2 \times 10^{-3}$ s^{-1}, one obtains an oscillatory response for $j = 1$ (i.e., positive h' and imaginary m) with very large vertical scales (order 200 km), using the branch of solutions associated with planetary or second class waves. For higher Hough modes, the solution becomes evanescent in the vertical but with relatively large vertical decay scales; for example, for $j = 9$, $m^{-1} \sim 30$ km. Thus, one expects to capture the essence of the response with a barotropic model, taken to represent in a general sense the vertically averaged solution.

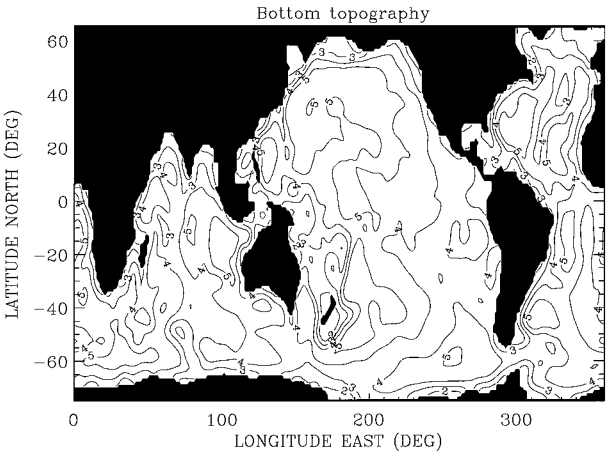

FIG. 2. Coastline geometry and bottom topography (in km) from Ponte (1993). Contour interval is 1 km.

Given a vertical scale m^{-1}, one can estimate whether an equilibrium or nonequilibrium response is expected. The relevant variable is sea level, which can be written as (Ponte 1992)

$$\zeta = \sum_j \frac{\zeta_j^{ib}}{1 + \phi_j} \tag{5}$$

with

$$\phi_j = \frac{N^2}{gm_j} \coth m_j H, \tag{6}$$

where ζ_j^{ib} is the equilibrium response for each Hough mode represented in the modal expansion of the forcing. Significant nonequilibrium response is expected only for values of ϕ different than zero, with resonances occurring for $\phi = -1$. For mode $j = 1$, expected to be the most strongly forced, we have $|m^{-1}| \sim 200$ km and $\phi \sim -4$. The response thus can deviate significantly from the IB value, both in amplitude and sign. For higher Hough modes, ϕ rapidly approaches zero and the IB solution holds.

In summary, for the large-scale high-frequency forcing under study, the theory strongly suggests the possibility for a nonequilibrium response, associated with the near-resonant excitation of the barotropic mode of the LTE. Furthermore, the occurrence of dynamic signals is somewhat sensitive to mode number. As higher Hough modes with shorter spatial scales are considered, the response rapidly becomes isostatic. Of course, in an ocean with bottom topography and coastal boundaries, the possibility for both local and global resonant excitation increases. The presence of land masses can also

influence the large-scale mass shifts necessary to attain an equilibrium response, as seen by Miller et al. (1993) in the case of the fortnightly tide signals in the tropical Pacific, and thus change the character of solutions in general. Such effects are explored next with a more realistic model.

3. Shallow-water numerical model

Given that the response to the 5-day, $s = -1$, Rossby–Haurwitz mode is likely to be depth-independent, the effects of realistic geometry and bottom relief are addressed using a barotropic numerical model. Stratification may nevertheless be important if bottom topography induces motions with short vertical scales (e.g., Willebrand et al. 1980). The scattering between barotropic and baroclinic motions in the presence of topography may indeed be a major dissipation mechanism for energy in the barotropic mode. Explicit treatment of this process is, however, beyond the scope of the present work.

Numerical experiments are performed with the shallow-water model in spherical coordinates described by Ponte et al. (1991) and Ponte (1993); the reader is referred to these earlier papers for details. The coastlines and bottom topography shown in Fig. 2 are those of Ponte (1993). The Arctic Ocean is closed off and a solid wall is assumed along latitude 65°N. A no-normal flow condition is imposed on all boundaries. The topography is necessarily smooth, given the 1.125° grid spacing. Focus is on the large-scale characteristics of the response. Although higher resolution might provide for more topographic wave resonances, these may not change significantly the structure of the open ocean response, apart from introducing small frequency shifts and splitting of the available basin-scale modes (Miller 1989). Dissipation is modeled as a linear drag term with variable coefficient b/H, where b is constant. Laplacian viscosity of the form given in Willebrand et al. (1980) is also included. A value of 1 g cm^{-3} is used for the density.

Most solutions discussed are obtained using the analytical pressure signal shown in Fig. 1, representative of the observed signal described by Madden and Julian (1972). We run the model from an initial resting state until periodicity in the solutions is achieved. Given the short period considered and the rapid barotropic adjustment, transients due to the initialization are insignificant after running the model for typically 70–100 days, depending on the amount of dissipation assumed. A number of different runs were performed to determine the dependence of the response on topography, coastal boundaries, dissipation, and forcing characteristics. These will be presented as the ensuing discussion warrants. Both lateral viscosity and bottom friction coefficients were varied. In all cases, for the large-scale signals studied here, the equivalent damping timescales due to lateral viscosity are much longer than those due to bottom friction, which is, therefore, the dominant dissipative mechanism.

4. Pressure-forced numerical solutions

To study the equilibrium or nonequilibrium character of the response in the numerical experiments, we need only focus on model sea level, which can in general be written as

$$\zeta = \zeta^{ib} + \zeta^{d}, \tag{7}$$

that is, the sum of IB and dynamic signals ζ^{ib} and ζ^{d}, respectively. Given a known pressure field, ζ^{ib} is defined by (1). The dynamic signal is the component of sea level that represents effective horizontal pressure gradients in the ocean (Gill 1982). In what follows, we will mostly be showing spatial maps of amplitude and phase of ζ and ζ^{d} signals at the 5-day period and a complex admittance or transfer function parameter defined as

$$\mathcal{A} = \frac{\rho g \mathcal{F}\{\zeta\}}{\mathcal{F}\{p_a\}}, \tag{8}$$

where $\mathcal{F}$ denotes the Fourier transform. An equilibrium response should yield an admittance of unit amplitude and phase equal to π, unless variability in $\overline{p_a}$ is comparable to p_a, which is not the case for the forcing in Fig. 1. Defining $\mathcal{A}$ as in (8) allows easy comparison with the gains and phases calculated by Luther (1982) and Woodworth et al. (1995) for Pacific and Atlantic tide gauges (see section 6); the phase convention is as in Luther; that is, positive phase means ζ leads p_a and vice versa.

The amplitude and phase of the 5-day signal in ζ are shown in Fig. 3 for the case of lateral viscosity coefficient equal to 10^8 cm^2 s^{-1}, and bottom friction coefficient $b = 0.1$ cm s^{-1}, which for a mean $H = 4000$ m is equivalent to an energy e-folding timescale of approximately 23 days, that is, weak dissipation compared to the maximum possible from the estimate of Luther (1982). As expected, the presence of boundaries and bottom topography introduces a whole spectrum of spatial scales and complex phase behavior, that is absent in the LTE solutions of the previous section. A number of features are worth noting. Sea level has larger amplitudes at high latitudes and a large-scale phase pattern of westward propagation (particularly in the Pacific) more or less consistent with the forcing in Fig. 1, but with significantly more structure than expected under a pure IB response. Westward phase propagation in the Pacific is not uniform and shows a tendency for latitudinal propagation near the boundaries. The North Atlantic shows westward and southward phase propagation. Inferred phase speeds are generally larger than that of the forcing.

The amplitudes of ζ^{d}, shown in Fig. 4, are not small compared to ζ^{ib} and confirm the importance of the dynamic response. The phase plot exhibits a complex behavior on the short scale, particularly in the Southern

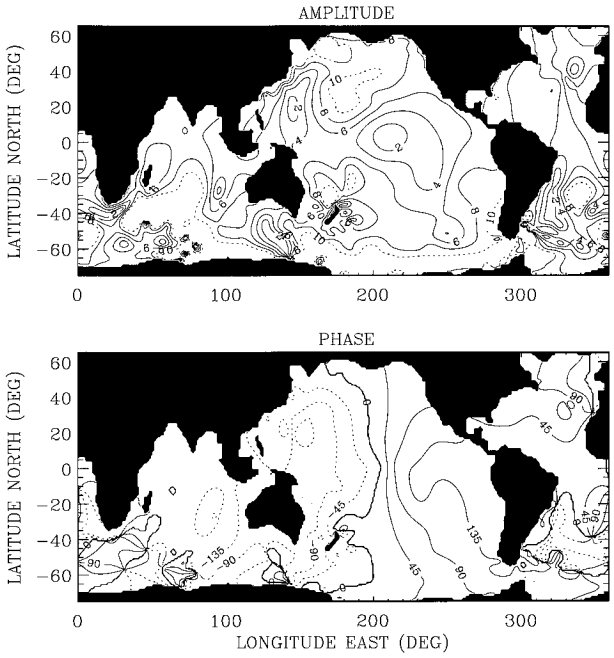

FIG. 3. Amplitude in millimeters and phase in degrees of model sea level at a period of 5 days for bottom friction coefficient $b = 0.1$ cm s^{-1}. Largest amplitude contoured is 10 mm (dotted line). Negative phases are plotted in dotted.

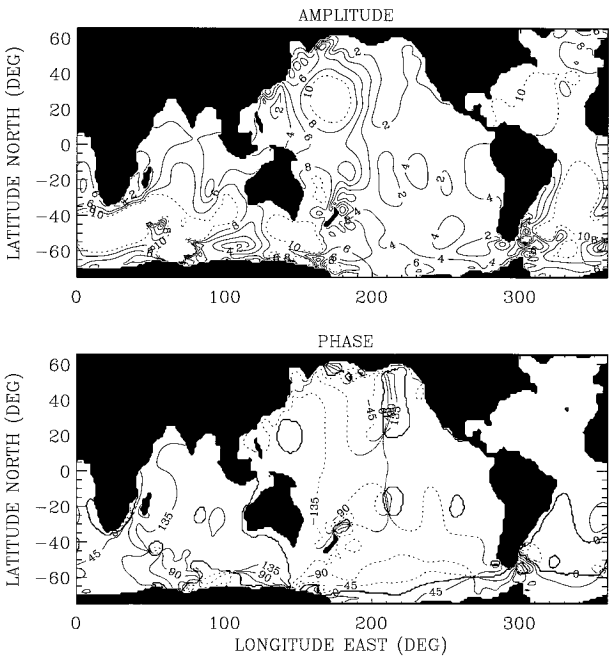

FIG. 4. Amplitude and phase of dynamic signal ζ^d for the solution given in Fig. 3. Plotting conventions are as in Fig. 3.

Ocean, showing several amphidromic points. However, the large-scale pattern is relatively simple, with regions of fairly homogeneous phase in the Atlantic, Pacific, and Indian Oceans and a tendency for the Atlantic Ocean to be approximately out of phase with large regions of the Pacific. There is some evidence of westward phase propagation in the North Pacific and somewhat amplified signals in the western half of the basin. These features are consistent with the excitation of Rossby wave energy. Comparison of the Pacific ζ^d patterns to the relevant mode structures described by Miller (1989) yields, however, no visible similarities.

The admittance $\mathcal{A}$ corresponding to the solution in Fig. 3 is shown in Fig. 5. Because p_a has amplitude constant in longitude and phase constant in latitude, the zonal structure in the amplitudes and the meridional structure in the phases of $\mathcal{A}$ are due to ζ and somewhat resemble those of Fig. 3. Amplitudes are generally different than one and phases are quite different than the constant value of π characteristic of the IB response. Large-scale patterns of sea level response both larger and smaller than the expected IB value are seen, but with the exception of a few small-scale localized features mainly in southern latitudes, admittance amplitudes are, in general, smaller than 2. For an approximately linear system, admittance amplitudes at or near an isolated resonant frequency should be inversely proportional to the friction coefficient (e.g., Munk and MacDonald 1960, p. 22). Solutions with $b = 0.02$ cm s^{-1} (dissipation five times weaker) did not yield significantly larger amplitudes. Solutions with stronger damping, discussed in more detail below, also did not lead to major changes in admittance amplitudes. Dependence on friction does not support the single resonance hypothesis. Results do not preclude, however, the existence

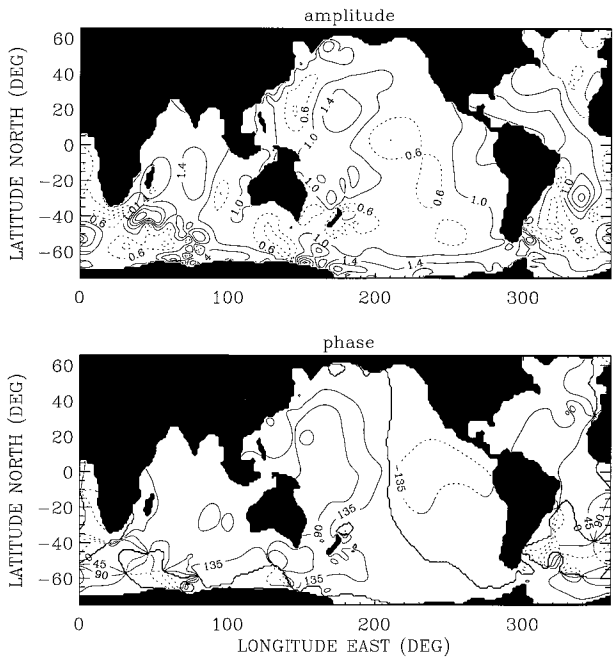

FIG. 5. Amplitude and phase of the admittance $\mathcal{A}$ defined by (8), calculated for the solution shown in Fig. 3. Solid lines denote amplitudes greater than one. Phase is plotted as in Fig. 3.

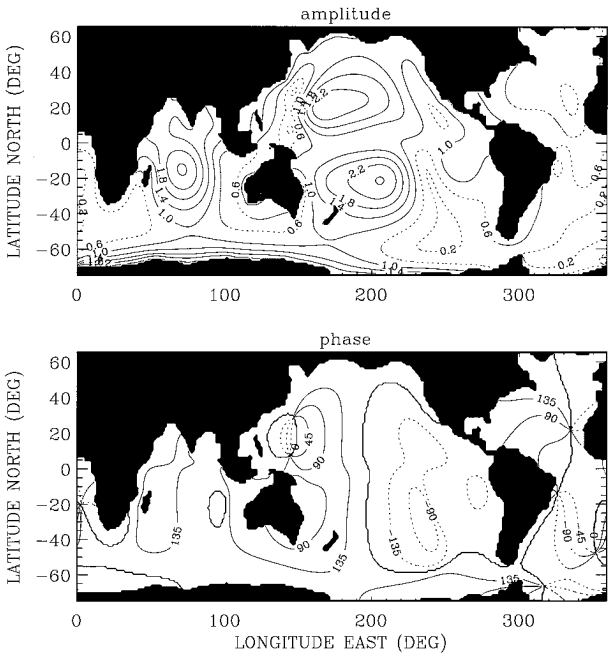

FIG. 6. Amplitude and phase of the admittance $\mathcal{A}$ for the case of a flat-bottom ocean with depth $H = 4000$ m. Plotting conventions are as in Fig. 5.

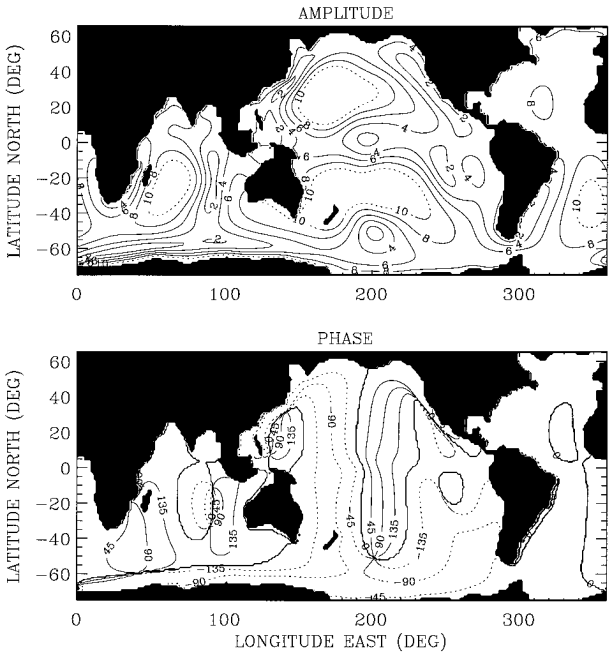

FIG. 7. Amplitude and phase of ζ^d for the case of a flat-bottom ocean with depth $H = 4000$ m. Plotting conventions are as in Fig. 3.

of several resonances closely spaced in frequency, in which case the dependence of $|\mathcal{A}|$ on friction should be weaker.

Resonant vorticity (local or basin) modes are most likely dependent on the vortex stretching induced by a varying topography. To check for these effects, Fig. 6 shows $\mathcal{A}$ for solutions with a flat-bottom ocean of depth $H = 4000$ m. Most local peaks in amplitude seen in southern latitudes in Fig. 5 disappear. The topography adds significant structure to the response, as expected because of distorted f/H contours, possibility of topographic waves, etc. Differences are also noticeable on the large-scale pattern, particularly in the Pacific, where larger admittance amplitudes, more symmetric pattern across the equator, and more rapid phase changes occur in the flat-bottom case. The alternating patterns of $|\mathcal{A}|$ larger and smaller than unity are, however, similar. In the Atlantic, the region where $|\mathcal{A}| > 1$ is smaller in Fig. 6, but the amphidromic structure is fairly similar in the two cases.

Figure 7 shows ζ^d for solution with constant H. Compared to the case with topography in Fig. 4, clear westward phase propagation is now present throughout the Pacific and also the South Indian Ocean. The amplitude and phase structure in the Pacific is highly reminiscent of the flat-bottom vorticity mode at period of 5 days calculated by Miller (1989; cf. Fig. 4d). The presence of topography inhibits this basin-scale Rossby wave excitation. Thus, to the extent that a basin-scale resonance may be contributing partially to the large-scale dynamic signals excited in the Pacific, topography actually leads to detuning and somewhat weaker excitation.[2] In the Atlantic, the phase is still approximately constant in Fig. 7, as in the case with topography. Regardless of topographic effects, large-scale Rossby wave excitation is apparently less efficient in the smaller Atlantic Ocean. Excluding southern features already noted, shorter-scale vorticity-type resonances related to the topography are not prominent in the solutions in Figs. 4 and 5. This is not due to strong damping of short scales by lateral viscosity in the model, as solutions with viscosity coefficients ten times smaller (not shown) were essentially unchanged, but may be related to the smooth topography used.

The solutions with $b = 0.1$ cm s^{-1} have an energy e-folding timescale approximately 10 times longer than the lower bound estimated by Luther (1982) from the observations. Figure 8 shows the admittance calculated with $b = 1$ cm s^{-1}, that is, for values of bottom friction approaching those necessary to achieve the maximum energy dissipation rates inferred by Luther. A number of effects are worth discussing in comparison with Fig. 5. Regions of large amplitudes are mostly suppressed and a cleaner large-scale pattern emerges. In the Atlantic, the localized peak off South America is largely damped out and there is a more general pattern of amplitudes smaller than one, with phase patterns quite similar to those in Fig. 5. In the Pacific, values larger than

[2] Miller (1989) draws some correspondence between the 5-day flat-bottom mode and a 5.5-day full topography mode (his Fig. 11c), but evidence for the excitation of the latter mode in our results is weak.

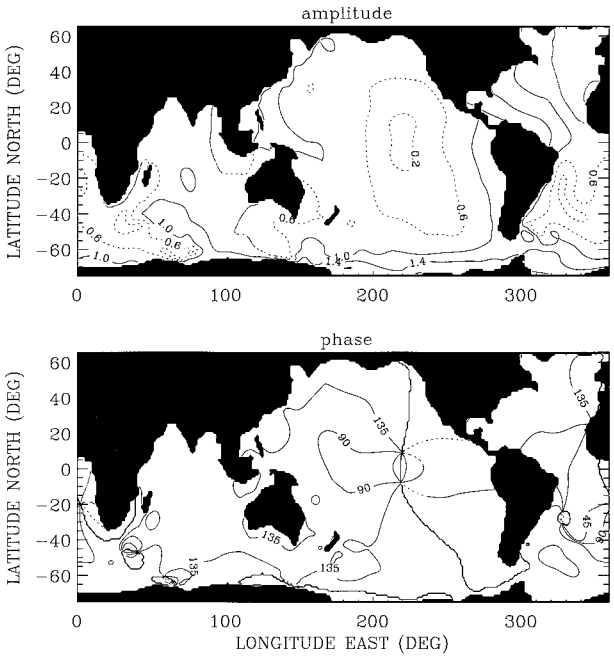

FIG. 8. Amplitude and phase of admittance $\mathcal{A}$ as in Fig. 5 but for the case of strong bottom friction ($b = 1$ cm s^{-1}).

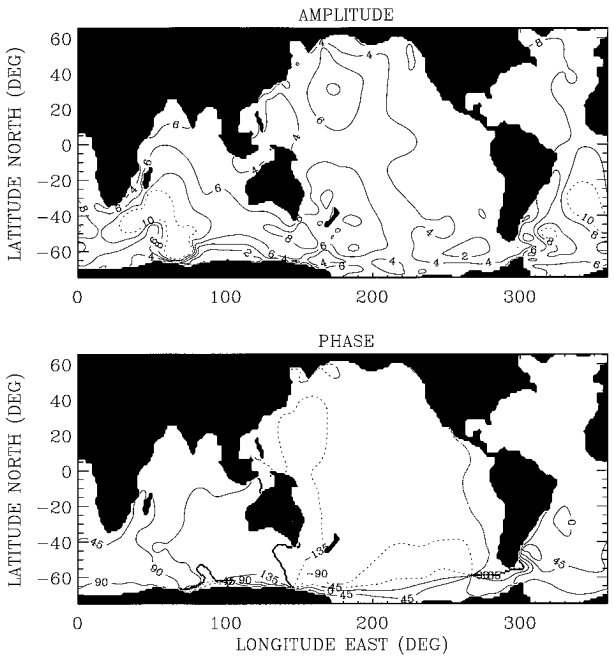

FIG. 9. Amplitude and phase of the dynamic signal ζ^d for solution with $b = 1$ cm s^{-1}.

one become more confined to the boundary regions. The phase still shows the same pattern with the addition of a couple of amphidromic points in the central Pacific. In the Indian Ocean, admittance amplitudes change from being larger to being mostly smaller than one in the highly damped solution. In general, there is a tendency for smaller admittance amplitudes, as expected for stronger damping (for infinitely large damping, one should approach a motionless, no sea level response).

The amplitudes and phase of ζ^d for $b = 1$ cm s^{-1}, shown in Fig. 9, can be compared with those in Fig. 4 for the weaker friction. Amplitude patterns are similar, although peak values are smaller and small-scale features are more damped out. Thus, the amplitude pattern becomes more homogeneous. Similarly, as most short-scale structure to the phase pattern disappears, the homogeneity of the large-scale phase of the ζ^d signal is quite clear. With the exception of the Southern Ocean, no clear phase propagation is apparent. The dynamic signals in the Atlantic and the Pacific are almost out of phase. The homogeneous amplitude and phase patterns over large portions of the Atlantic, Indian, and Pacific Oceans, again excluding the Southern Ocean, imply basin-scale dynamic pressure gradients that are, for the most part, small compared to the imposed forcing pressure gradients (e.g., see Fig. 1). These results are robust to changes in the lateral viscosity coefficient; solutions are virtually unchanged when viscosity is set to zero.

As another test of the importance of resonances for the dynamic response, one can force the model at different frequencies. In case of a single resonance, one expects a substantial change in the response as the forcing frequency changes. A more equilibrium-like solution should result away from resonance. If several closely spaced resonant frequencies are present, the modes in Miller (1989) suggest that one should still see changes in the spatial patterns, by changing the frequency across the resonant band. Figure 10 shows ζ^d calculated from

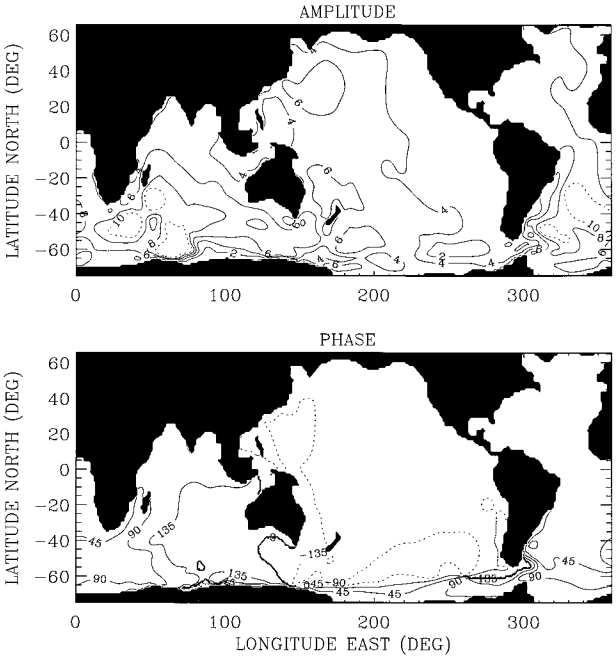

FIG. 10. Amplitude and phase of admittance $\mathcal{A}$ as in Fig. 8 but for the case of forcing at a period of 6 days.

solutions forced with a pressure wave of period equal to 6 days. Comparison with Fig. 9 reveals very little differences between the cases with 5-day and 6-day forcing. Solutions found for periods of 4, 4.5, and 5.5 days (not shown) exhibited similar behavior. The weak dependence of the large-scale ζ^d pattern on frequency does not indicate a major role of basin or global resonances on the nonequilibrium response, at least in the case of high dissipation. In the case of weaker dissipation, changes with frequency are more apparent, but mostly at the short scales.

5. Interpretation

The numerical solutions and their dependence on frequency, topography, and friction suggest a plausible interpretation for the nature of the nonequilibrium response to the 5-day atmospheric Rossby–Haurwitz wave. Leaving out localized features, which appear to be most prominent in the Southern Ocean (south of ~40°S), and keeping our focus on the basin-scale features, two basic mechanisms seem to be at work. First, there is the near-resonant excitation of vorticity-type modes or waves, as discussed by Luther (1982) and Miller (1989) for the Pacific. The importance of such near-resonances for the Pacific response is clear in solutions with a flat bottom but, as discussed above (see also Luther 1982), diminishes when realistic topography is considered and is more apparent in the western part of the basin. For damping rates approaching maximum values inferred by Luther, the influence of such signals is further reduced. In the Atlantic, north of ~20°S, the presence of free vorticity modes seems unimportant, even for a flat-bottom ocean. The second mechanism responsible for the basin-scale nonequilibrium signals has to do with the interbasin adjusment of the mass field under gravity (e.g., Miller et al. 1993) and needs a more detailed discussion.

Given the structure of the forcing, an IB solution involves not only intrabasin but also interbasin mass fluxes. Intrabasin adjustment of mass field is easier to establish given the smaller distances involved. In fact, the solutions suggest the intrabasin adjustment is close to equilibrium, in the sense that $\nabla\zeta^d$ is small compared to $\nabla\zeta^{ib}$. Interbasin fluxes have to be accomplished through the Southern Ocean. These fluxes are nonlocally driven and depend on free wave propagation to be established. A number of factors may preclude total adjustment to equilibrium. For example, forcing scales may be such that only a horizontally trapped response is possible. Note that, in this case, it is the lack of appropriate free waves, rather than their resonant excitation, that may lead to departures from IB solution. When propagation is possible, friction may still lead to horizontal trapping. The presence of boundaries and constricted geometries may also introduce the possibility of Helmholtz-type resonances (e.g., LeBlond and Mysak 1989), as discussed by Gotlib et al. (1987) and Marchuk and Kagan (1989) for the global ocean.

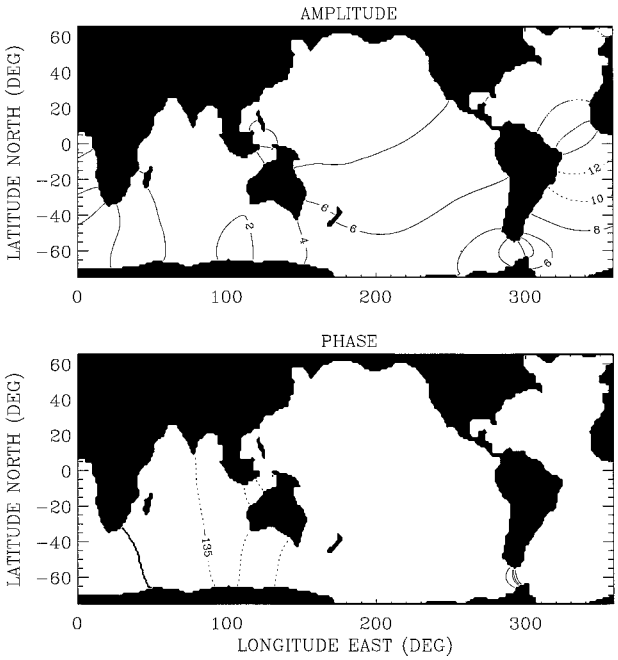

FIG. 11. Amplitude and phase of the dynamic signal ζ^d as in Fig. 9 but for the solution with no rotation.

Gravity waves (including Kelvin waves) should play a more prominent role in the interbasin mass adjusment processes than vorticity (Rossby) waves: They propagate faster and are more efficient at transporting mass due to their larger potential to kinetic energy ratios relative to Rossby waves (e.g., Gill 1982). One way to check for the relevance of mass adjustment processes to the nonequilibrium response in our solutions is, therefore, to run the model without rotation, in which case all vorticity modes are filtered out. Figure 11 shows ζ^d calculated as in Fig. 9 but with no rotational effects. The response is still far from equilibrium. The pattern of homogeneous phases in the Atlantic and Pacific is striking. Furthermore, the two oceans oscillate mostly out of phase, with a sharp phase shift across Drake Passage, where a node in amplitude is also apparent. The Indian Ocean plays somewhat of a transitional role. Most of these features are discernable in the response with rotation (cf. Fig. 9), although close correspondence between the two solutions is not expected, given that the presence of rotation not only adds vorticity waves to the problem but also changes the gravity wave spectrum. Thus, the importance of gravity wave dynamics and interbasin mass adjustment processes seems clear in our solutions.

The reasons for the partial interbasin adjustment and the large-scale nonequilibrium response in our solutions, in particular the role of resonances, remain an interesting issue. As discussed by Marchuk and Kagan (1989), the global oceans support a pure gravitational mode at a period of about 114 h. Such a mode may play a role in the solution in Fig. 11, in which the Atlantic and Pacific resemble a co-Helmholtz oscillator. Similar runs without rotation, but

TABLE 1. Gain and phase values for the island stations reported by Luther (1982) and Woodworth et al. (1995) (see text for explanation) and respective model-based values for weak friction (wf) and strong friction (sf) cases, with $b = 0.1$ and 1 cm s^{-1}, respectively.

	Data		Model (wf)		Model (sf)	
Stations	Amp	Phase	Amp	Phase	Amp	Phase
Balboa	1.31 ± .31	−170 ± 11	1.42	−140	1.1	−132
Galapagos	1.16 ± .34	−150 ± 14	1.38	−132	1.06	−124
Canton	0.36 ± .17	137 ± 41	0.87	91	0.72	80
Majuro	0.57 ± .37	79 ± 44	1.39	70	0.94	85
Kwajalein	0.56 ± .19	117 ± 19	1.38	65	0.93	87
Eniwetok	0.51 ± .26	140 ± 29	1.26	56	0.85	92
Truk	0.63 ± .16	132 ± 14	0.72	72	0.88	111
Yap	0.83 ± .40	148 ± 23	0.72	133	1.08	133
Guam	0.63 ± 0.18	140 ± 14	0.29	106	0.80	128
Wake	0.43 ± 0.18	120 ± 22	1.46	60	0.80	89
Johnston	0.37 ± .36	41 ± 61	1.32	129	0.74	104
Pago Pago	0.79 ± .24	114 ± 28	1.34	109	0.72	92
Hilo	0.57 ± .13	162 ± 11	0.90	172	0.45	127
Honolulu	0.44 ± .09	159 ± 8	0.99	165	0.51	127
Midway	0.95 ± .15	161 ± 7	1.16	129	0.68	117
Ascension	0.25 ± .13	−38	1.06	19	0.82	17
St. Helena	0.14/0.71	−38/−82	0.57	66	0.46	23

varying the forcing period over the 4–6 day band, indicate a possible resonance between 4 and 5 days, consistent with the results reported by Marchuk and Kagan. Unfortunately, the spatial structure of their mode has not been published and comparison with our results is not possible. When rotation is added, Marchuk and Kagan report no mode at 114 h, but instead another mode at slightly shorter period (112 h). The structure of this mode is discussed by Gotlib et al. (1987). They draw a correspondence between the 114 h (no rotation) and 112 h (with rotation) modes and assert the gravitational nature of the 112-h mode, but it is clear from their discussion that the two modes have very different spatial structure and that effects of rotation are thus important. In any case, the ζ^d solutions in Figs. 4 and 9 show some similarities with the structure of the 112-h mode in Gotlib et al. (e.g., fairly constant amplitude and phase in the North Atlantic, similar features in Southern Ocean), but the details are very different. The extent to which such a mode influences our solutions is thus not clear.

TABLE 2. Phase differences between sea level at island stations reported by Luther (1982) and respective model-based values for weak friction (wf) and strong friction (sf) cases, with $b = 0.1$ and 1 cm s^{-1}, respectively.

Stations	Luther	Model (wf)	Model (sf)
Honolulu/Balboa	126 ± 33	−132	−176
Canton/Balboa	73 ± 26	142	123
Kwajalein/Canton	−13 ± 17	−43	−12
Truk/Kwajalein	−8 ± 13	−12	8
Eniwetok/Canton	0 ± 27	−58	−13
Yap/Truk	−11 ± 19	45	10
Guam/Kwajalein	0 ± 15	19	16
Guam/Eniwetok	−40 ± 26	30	20
Guam/Wake	−26 ± 16	22	18
Wake/Johnston	−31 ± 22	−89	−37
Kwajalein/Honolulu	−98 ± 29	−135	−74
Johnston/Hilo	−49 ± 24	−60	−36
Canton/Honolulu	−52 ± 22	−89	−60
Canton/Hilo	−62 ± 26	−99	−62
Kwajalein/Pago Pago	−25 ± 33	−60	−24
Pago Pago/Hilo	−27 ± 36	−82	−50

The interplay of the two mechanisms described above (i.e., vorticity-type resonances and mass adjustment processes, of either a resonant or off-resonant nature) leads to the nonequilibrium signals in the model solutions. The latter mechanism seems to play a significant role for regions other than the Southern Ocean (especially for the Atlantic), and more so when high damping rates are considered. Excitation of vorticity modes adds structure to the phase and amplitude patterns of dynamic signals, particularly in the Southern Ocean and in the western Pacific, and more so the weaker the dissipation.

6. Comparison with observations

The model solutions predict a large-scale structure for $\mathcal{A}$ that can be tested against the Pacific and Atlantic tide gauge calculations reported by Luther and Woodworth et al. and discussed in the introduction. One can interpret the model results as a pure signal in the sense that we have filtered out any wide band noise and nonstationarity in the forcing. The predicted signal could then be in error due to either poor quality of the assumed forcing wave or to model errors per se. As for the observations, the gain and phase values are obtained over various different periods, involving some degree of nonstationarity, and contain noise associated with the presence of wide band forcing in wavenumber (instead of the single wavenumber constituting the signal) and in frequency. For these reasons, the comparison presented here is only qualitative.

The observed gain and phase values are reproduced in Table 1. The values for the Pacific, taken from Table 2 of Luther, are representative of the 4–6 day band, while those for the Atlantic were kindly provided by

P. Woodworth (1996, personal communication; see also Woodworth et al. 1995) and represent the 4–5-day band. Results for St. Helena showed some dependence on the particular record periods considered in the analysis (Woodworth et al. 1995); we show in Table 1 the observed range of gain and phase values. Otherwise, error bars at the 95% confidence level are given. Table 1 also includes corresponding gain and phase values calculated from the model solutions with ''weak'' ($b = 0.1$ cm s^{-1}) and ''strong'' ($b = 1$ cm s^{-1}) friction for the forcing shown in Fig. 1, which most closely resembles the observed wave. Table 2 presents a similar comparison between the sea level phase differences between various station pairs presented in Table 4 of Luther and respective values calculated from the model.

The agreement between model and data inferred from Tables 1 and 2 is qualitatively good for both weak and strong friction cases, but is somewhat improved in the latter, with phases and gains closer to the observed values in general. In particular, gains larger than one in the central Pacific present in the weak friction solution (Fig. 5) become smaller than one in the strong friction case, providing better agreement with observations at Majuro, Kwajalein, Eniwetok, Johnston, and Pago Pago. With the exception of Yap, the strong friction solution thus reproduces well the observed local tendencies for 1B undershoot and overshoot. The tendency for an in-phase relation between sea level and pressure observed in the Atlantic (St. Helena and Ascension) is also correctly predicted by the model.

Output from 1-yr long model runs described in Ponte (1993) and Gaspar and Ponte (1997), performed with realistic operationally derived pressure fields, provided an opportunity to check effects of wide band noise, nonstationary signals, etc., on the comparisons. Results (not shown) indicate always a clear tendency for a nonequilibrium response, but the admittance values may differ from those of Table 1. Agreement improves for certain stations and worsens for others (see also Fig. 10 of Ponte 1993). Note that the extent to which the observed 5-day pressure signal is captured in the operationally analyzed fields is not well known, although Weber and Madden (1993) have presented evidence for such a signal in the European Centre for Medium-Range Forecasts fields. Weber and Madden also find evidence for seasonal modulation of the pressure signal (strongest in spring and autumn). In light of the likely importance of noise and nonstationarity in the forcing when determining local admittance functions, a more quantitative model and data comparison must use realistic forcing pressure fields for longer (several years) and concurrent periods, and deal carefully with the issue of seasonality.

7. Summary and final remarks

The simple experiments in this study confirm the nonisostatic nature of the response to loading found by Luther (1982) and Woodworth et al. (1995) at periods close to 5 days. The qualitative comparisons with the observations in the Pacific and Atlantic indicate that the observed non-IB signals are most likely related to the Rossby–Haurwitz 5-day atmospheric mode, and favors a highly damped oceanic response. The dependence of solutions on frequency and topography, their behavior under different damping rates, and the amplitude and phase patterns of dynamic signals suggest that, besides the near-resonant excitation of large-scale vorticity modes, whose effects are substantially reduced when topography and strong damping are present, the large-scale nonequilibrium response is due to gravity wave dynamics and related processes of adjustment of the mass field. The inability to shift mass among the different oceans at the rate needed for global equilibrium response is not surprising, given that the timescale for barotropic adjustment of the global ocean, relevant for the spatial scales of the Rossby–Haurwitz pressure wave considered, is not negligible compared to forcing period.

Large-scale nonequilibrium signals were a general characteristic of several numerical experiments forced by p_a fields with scales similar to the observed Rossby–Haurwitz atmospheric wave. These included forcing the model with zonal wavenumber $s = -2$ and $s = 1$ (eastward propagating) disturbances, and higher Hough mode numbers. The model responded nonisostatically even when the LTE solutions predict otherwise for a given forcing structure. Other important differences between numerical and analytical solutions are also clear. For example, the phase between ζ and p_a is not confined to values of π or zero, and the phase between ζ at different longitudes is not simply that of the forcing wave, as one would expect from the LTE solutions (5) in the case of an aquaplanet. Friction, topography, and landmasses can all contribute to the increased complexity of the numerical solutions, by introducing many spatial scales and zonal dependences far from having the simple form $e^{is\psi}$, and by changing wave characteristics and ultimately affecting the adjustment timescales. Thus, although analytical solutions give an indication of what the response will be like, solving the problem numerically is ultimately required.

The strongly damped solutions reproduce more closely the observations and largely smooth out some of the shorter-scale likely unrealistic features associated with local resonances. Whether such high damping rates are realistic or appropriate everywhere remains an issue. The strong dissipation inferred by Luther is based on the single resonance hypothesis and the width of the spectral peaks for a couple of tide gauge records in the western Pacific. It is, however, true that similar values of dissipation have been inferred for the diurnal and semidiurnal tides. The mechanisms responsible for the dissipation are also unclear, although scattering into baroclinic motions by bottom topography is a strong candidate. Proper parameterization of such processes, here simply done with a depth-dependent linear drag law,

may be important for more quantitative data and model comparisons in the future.

The model, of course, predicts the admittance function globally and offers the opportunity for comparison with other tide guages and possibly altimeter data. The estimation of $\mathcal{A}$ from altimeter data is made difficult by the short period of the oscillation relative to the repeat period of altimeters such as TOPEX/Poseidon (10 days). The large spatial scales of the dynamical signal (e.g., Fig. 9) may allow subsampling to create a time series of global maps with sufficient resolution. More powerful methods involving data assimilation could also be tried. Whether the sea level signal (typical amplitudes of 0.5 cm according to Fig. 9) is strong enough to be detectable in the data remains a question, however. Alternatively, many island tide gauges remain to be examined, and analysis of Pugh (1979) for the Indian Ocean shows that peculiar sea level behavior at 5-day periods is not confined to the Pacific and Atlantic Oceans.

We have purposefully used deterministic forcing in our solutions to examine the response to the Rossby–Haurwitz mode in isolation from any ''noise.'' Of course the real forcing is stochastic, and the nature of the response may differ under such forcing. In particular, nonequilibrium signals related to interbasin mass adjustment processes may not be as important when the pressure signals do not have, for example, a perfect $s = -1$ structure. Analysis of the response in runs with realistic forcing are needed to clarify these issues, as discussed in section 6.

Finally, we return to the issue of resonant excitation of global or basin modes. The identification in the model solutions of the modes calculated by Miller (1989) for the Pacific or Gotlib et al. (1987) for the global ocean was not very successful. This may signify that the Rossby–Haurwitz forcing wave does not project strongly onto these modes. Another reason for the poor match between the detailed spatial structures of the modes and our solutions could be the effects of friction and dissipation. These effects may lead to stronger attenuation of some features of the modal structure compared to others. For example, bottom friction acts more strongly on shallow depths, and thus influence of some topographic features on the mode may be weakened. Vorticity and gravity wave components involved in the modes may be differently affected. The effects of friction on the structure of the modes of Miller (1989) or Gotlib et al. (1987) need to be addressed before this issue can be resolved.

Acknowledgments. The author has greatly benefitted from exchanges with D. Luther, G. Kivman, R. Madden, A. Miller, P. Woodworth, and C. Wunsch, which led to a number of clarifications in the interpretation of the results and a much improved manuscript. This work was carried out while the author held a visiting appointment of Physicien Associé at the Groupe de Recherche de Géodésie Spatiale of the Observatoire Midi-Pyrénnées. The support of OMP and the hospitality of its staff is gratefully acknowledged.

REFERENCES

Fu, L.-L., and G. Pihos, 1994: Determining the response of sea level to atmospheric pressure forcing using TOPEX/POSEIDON data. *J. Geophys. Res.,* **99,** 24 633–24 642.

Gaspar, P., and R. M. Ponte, 1997: Relation between sea level and barometric pressure determined from altimeter data and model simulations. *J. Geophys. Res.,* **102,** 961–971.

Gill, A. E., 1982: *Atmosphere–Ocean Dynamics.* Academic Press, 662 pp.

Gotlib, V. Yu., B. A. Kagan, and G. A. Kivman, 1987: On the lowest gravitational mode of eigen oscillations in the world ocean: Part 2. *Sov. J. Phys. Oceanogr.,* **1,** 11–16.

Groves, G. W., and E. J. Hannan, 1968: Time series regressions of sea level on weather. *Rev. Geophys.,* **6,** 129–174.

Holton, J. R., 1975: *The Dynamic Meteorology of the Stratosphere and Mesosphere. Meteor. Monogr.,* No. 37, Amer. Meteor. Soc., 218 pp.

LeBlond, P. H., and L. A. Mysak, 1989: *Waves in the Ocean.* 3d ed. Elsevier, 602 pp.

Longuet-Higgins, M. S., 1968: The eigenfunctions of Laplace's tidal equations over a sphere. *Philos. Trans. Roy. Soc. London, Ser. A,* **262,** 511–607.

Luther, D. S., 1982: Evidence of a 4–6 day barotropic, planetary oscillation of the Pacific Ocean. *J. Phys. Oceanogr.,* **12,** 644–657.

——, 1983: Why haven't you seen an ocean mode lately? *Ocean Modelling,* (unpublished manuscript), **50,** 1–6.

Madden, R. A., and P. R. Julian, 1972: Further evidence of global-scale, 5-day pressure waves. *J. Atmos. Sci.,* **29,** 1464–1469.

Marchuk, G. I., and B. A. Kagan, 1989. *Dynamics of Ocean Tides* (translated from Russian). Kluwer, 327 pp.

Miller, A. J., 1986: Nondivergent planetary oscillations in midlatitude ocean basins with continental shelves. *J. Phys. Oceanogr.,* **16,** 1914–1928.

——, 1989: On the barotropic oscillations of the Pacific. *J. Mar. Res.,* **47,** 569–594.

——, D. S. Luther, and M. C. Hendershott, 1993: The fortnightly and monthly tides: Resonant Rossby waves or nearly equilibrium gravity waves? *J. Phys. Oceanogr.,* **23,** 879–897.

Munk, W. H., and G. J. F. MacDonald, 1960: *The Rotation of the Earth.* Cambridge University Press, 323 pp.

Ponte, R. M., 1992: The sea level response of a stratified ocean to barometric pressure forcing. *J. Phys. Oceanogr.,* **22,** 109–113.

——, 1993: Variability in a homogeneous global ocean forced by barometric pressure. *Dyn. Atmos. Oceans,* **18,** 209–234.

——, D. A. Salstein, and R. D. Rosen, 1991: Sea level response to pressure forcing in a barotropic numerical model. *J. Phys. Oceanogr.,* **21,** 1043–1057.

Pugh, D., 1979: Sea levels at Aldabra Atoll, Mombasa and Mahé, western equatorial Indian Ocean, related to tides, meteorology and ocean circulation. *Deep-Sea Res.,* **26A,** 237–258.

Weber, R., and R. A. Madden, 1993: Evidence of traveling external Rossby waves in the ECMWF analyses. *J. Atmos. Sci.,* **50,** 2994–3007.

Willebrand, J., S. G. H. Philander, and R. C. Pacanowski, 1980: The oceanic response to large-scale atmospheric disturbances. *J. Phys. Oceanogr.,* **10,** 411–429.

Woodworth, P. L., S. A. Windle, and J. M. Vassie, 1995: Departures from the local inverse barometer model at periods of 5 days in the central South Atlantic. *J. Geophys. Res.,* **100,** 18 281–18 290.

Wunsch, C., and D. Stammer, 1997: Atmospheric loading and the oceanic ''inverted barometer'' effect. *Rev. Geophys.,* **35,** 79–107.